RESEARCH ARTICLE

Anatomic study of carpal tunnel in adults using monoenergetic reconstruction of dual-energy computed tomography

Heng Zhao,[1] Fei Peng,[2] De-Qiu Tang,[3] Jin-Cai Liu,[4] Hao Lei,[5] Qiang Liu,[6] Fang Wang,[7] Qiu-Ping Ren,[8] Jiao Yang Li,[9] Feng-zhe Wang,[10] Zhao Lu,[11] Shi Nong Pan[12]

Abstract

Objective: To seek optimal keV settings for imaging carpal tunnel in adults by dual-energy computed tomography (DECT) monoenergetic technique; to describe anatomic characteristics of carpal tunnel and to observe correlation between carpal bony and soft tissue structures.

Methods: DECT images of 20 wrists (11 left and 9 right wrists; 14 men, mean age 26.93±1.38 years, range 23 to 28, and 6 women, mean age 24.17 ± 0.98 years, range 23 to 26) were evaluated. Monoenergetic images were reconstructed at 42, 62, 82, 102, 122, and 142 keV. Image quality was assessed along a 5-point Likert scale, and the highest-quality images were chosen for quantitative analysis. Two musculoskeletal radiologists performed both analyses independently.

Results: The optimal energy spectrum with the best contrast-to-noise ratio (CNR) for monoenergetic images were at 62 keV (19 wrists, 95%) and 61 keV (1 wrist, 5%). There was substantial interobserver agreement between the readers in the 5-point Likert scale analysis of image quality (k= 0.793). Bland-Altman plots also indicated good agreement between observers in quantitative analysis. Intra-category 1 and 2 correlation was mostly discovered at hamate hook level and middle level of pisiform ($P < 0.05$), while bony and soft tissue structures partly reached correlation ($P < 0.05$).

Conclusion: The optimal energy spectrum for monoenergetic DECT imaging of carpal tunnel structures was 62 keV. DECT monoenergetic imaging could predict changes in soft tissue structures and demonstrate carpal tunnel anatomic structures.

Keywords: DECT, monoenergetic, keV, carpal tunnel, anatomy. (JPMA 71: 663; 2021)

DOI: https://doi.org/10.47391/JPMA.1203

Introduction

The anatomy of carpal tunnel is complex, and inflammation of internal structures can easily elevate intra-carpal tunnel pressure, leading to entrapment of median nerve (MN) and development of carpal tunnel syndrome (CTS). CTS causes pain and paresthesias, and severe cases may result in deformity and disability of the upper extremity.[1]

Magnetic resonance imaging (MRI) has demonstrated superiority in imaging of soft tissues and bony structures of carpal tunnel, and provides high-quality images,[2] but clinical application of MRI might be limited because of time constraints or contraindications. Ultrasound is an effective, noninvasive, non-radioactive method of examination that is comparable to MRI in terms of resolution of soft tissues of carpal tunnel region.[3] However, ultrasound cannot penetrate bones or depict lesions of deep bony tissues, thus limiting overall diagnostic efficacy for diseases of musculoskeletal system. Traditional computed tomography (CT) is well known for advantages such as rapid scanning and few contraindications, and single energy CT (SECT) has proven incomparable in evaluation of bony structures of carpal tunnel. SECT readily displays bony abnormalities and conditions associated with bony deformities that occupy carpal tunnel space. SECT can accurately predict bony etiology, location, and extent of carpal tunnel stenosis through thin axial images, multiplane reformation, and 3D reconstruction.[4] However, the resolution of SECT for display of soft tissues is poor, and it is usually only applicable when bony structure damage or injury is suspected.[5]

DECT has inherited the advantages of SECT for display of bony structures, and it offers better resolution of soft tissues, allowing for better visualization of soft tissue structures such as tendons and ligaments.[6] DECT imaging incorporates information from low- and high-energy data that are synchronously acquired during a single scan,[7]

[1,6,11,12]Department of Radiology, Shengjing Hospital of China Medical University, Heping, Shenyang, [2-5,7,8]Department of Radiology, [9]Department of Metabolism & Endocrinology, The First Affiliated Hospital of University of South China, Hengyang, Hunan, [10]Department of Radiology, The 4th People Hospital of Shenyang, Huanggu, Shenyang, China.

Correspondence: Shi Nong Pan. Email: cjr.panshinong@vip.163.com

and DECT workstation offers several post-processing techniques, including production of virtual monoenergetic images that can be generated at any desired energy level; the CNR of these virtual images can be optimized for significantly improved image quality.[8] However, as yet, there are no published reports regarding application of monoenergetic DECT imaging for carpal tunnel.

Our purpose was to assess monoenergetic DECT imaging of carpal tunnel in adults and seek the optimal energy spectrum, to further understand anatomic characteristics of internal carpal structures and the correlation between carpal bony and soft tissue elements.

Materials and Methods

This study gained the approval from the Medical Ethic Committee of University of South China. Between January 2016 and February 2017, we sequentially chose 24 young adult patients (range 23 to 28 years) with acute single wrist trauma and suspicion of bony injury on initial CT scan, after gaining informed consent form the patients, DECT was performed on normal contralateral wrist(uninjured) for comparison, so as to judge the suspected bony injury. Hence we obtained 24 normal (uninjured) adult wrists and included them for initial study. After monoenergetic reconstruction of DECT data, wrists with bifid median nerve (MN) (n=2) and poor-quality images (n=2) were excluded. Thus, final analysis included 20 normal(uninjured) wrists (11 left wrists and 9 right wrists) from 14 men (average age 26.93 ± 1.38 years; range 23 to 28 years) and 6 women (average age 24.17 ± 0.98 years; range 23 to 26 years) (Figure-1).

Scanning was performed with a 256 row dual source CT (Somatom Definition; Siemens, Germany). A dual source mode was applied to CT scanning (collimation, 64×0.6 mm; pitch, 0.7; rotation time, 0.33 sec) with patients prone and wrists in resting position. The tube voltages were set as 80 kVp (tube A) and 140 kVp (tube B). The predefined tube current-time was configured for 2:1 ratio, with effective mAs of tube A and tube B were 220 and 110, respectively.

Each DECT scanning generated three different sets of images, included 80kVp, 140 kVp and weighted average (120 kVp). Three corresponding sets of transverse images with 0.6 mm section thickness were reconstructed.

The acquired data were post-processed using dedicated dual-energy monoenergetic software on a Siemens workstation (SyngoMMWP VE40B). First, we outlined a

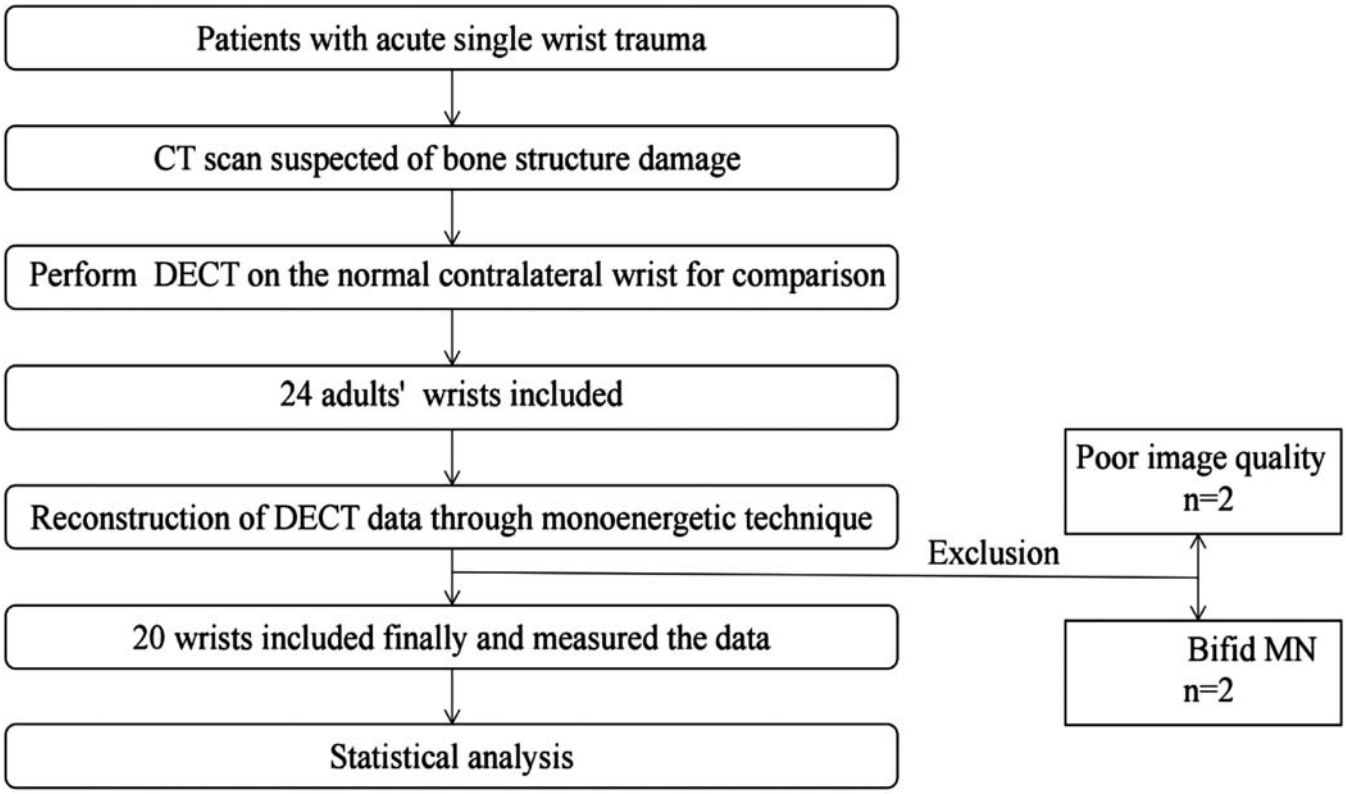

Figure-1: Flowchart shows inclusion and exclusion criteria for the study.

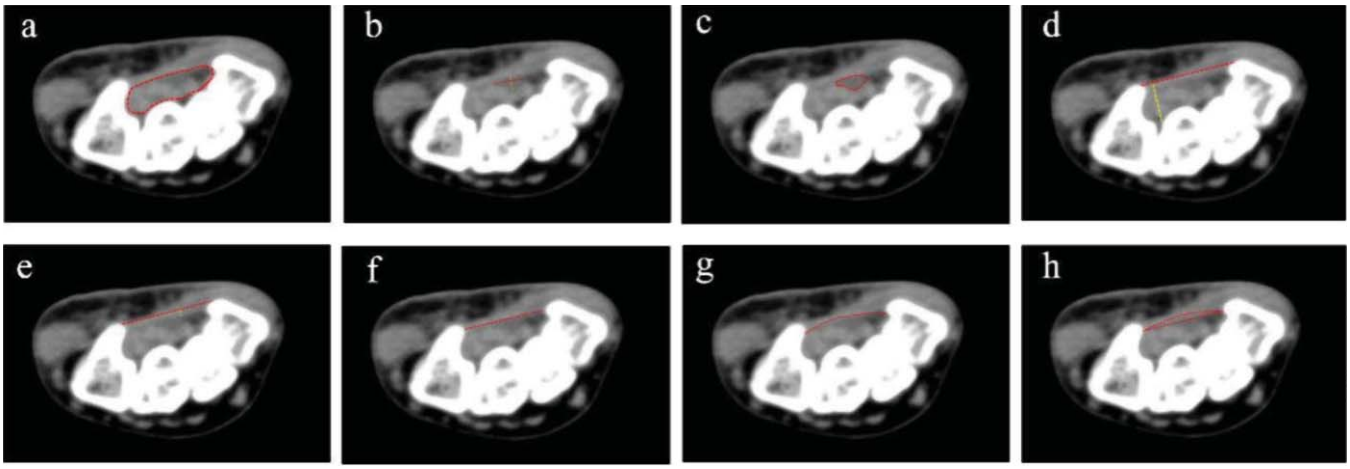

Figure-2: (a) The area of red dotted outline means the CSA of the carpal tunnel. (b) The red dotted line means the long axis of MN, the yellow dotted line means the short axis of MN. (c) The area of red dotted outline means the CSA of MN. (d) The red dotted line means the width of carpal tunnel bony structures, the yellow dotted line means the depth of carpal tunnel bony structures. (e) A red dotted line drawn from the tip of the hamate hook to the region of the trapezial tubercle, the vertical distance (the yellow dotted outline) between the top of TCL and red dotted line means the bowing of TCL. (f) The red dotted line means CAW. (g) The red dotted outline means the CAL. (h) The area of red dotted outline means the CAA.

region of interest (ROI) in the soft tissue structure area of carpal tunnel, after which, through a monoenergetic technique, corresponding optimal spectrum with the best CNR was obtained. Monoenergetic images were then reconstructed respectively at six energy values separated by 20 keV increments.[10]

Two musculoskeletal system radiologists (with 4 and 16 years of experience, respectively) evaluated the image quality independently. We scored image quality along Likert Scale, with 1, poor; 2, adequate; 3, average; 4, good; and 5, excellent.[11]

We chose the highest quality (Likert score 5) images for objective analysis. Four levels of the wrist were identified. The first level was proximal section at distal radioulnar joint was seen. The second level was located in middle of pisiform, which represented entrance of carpal tunnel. The third level was situated at hamate hook (middle part of carpal tunnel). The fourth level was placed at the point where proximal metacarpal bones became visible. The measurements are shown in Figure-2. The same two radiologists measured the image data independently.

Taking optimal energy spectrum settings ratio $\geq$ 70% as basic requirement, 95% of the 62 keV settings ratio as research data, power (1-β) set at 0.80 and α = 0.05 (one side). Sample size was calculated by the formula $n = (\mu\alpha+\mu\beta/\delta)^2\alpha\pi_0(1-\pi_0)$.[9] In total, minimum sample size was 20. In subjective analysis of Likert Scale images, Cohen's kappa (κ) was used to verify consistency between the two observers. In objective image analysis, Bland-Altman plots were presented to demonstrate the level of agreement between two independent readers. The numerical values measured at four levels were analyzed by using one-way ANOVA and Pearson correlation. The difference was statistically significant at $P < 0.05$. SPSS Version 17.0 and Medcalc Version 17.8 were used for statistical analysis.

Results

In 20 wrists, the optimal energy spectrum with the best CNR on monoenergetic images was 62keV (19 wrists, 95%); one wrist showed the best quality at 61keV. All monoenergetic images were reconstructed at 42, 62, 82, 102, 122, and 142 keV (Figure-3), and Likert scores confirmed that reconstructions at 62 keV had highest quality. The overall interobserver agreement for Likert scale grading was substantial (κ = 0.793).

The means ± standard deviations (SD) of cross-sectional area (CSA) of carpal tunnel, CSA of MN, the long axis and short axis of MN, swelling ratio (CSA of MN at the pisiform bone level/CSA of MN at distal radioulnar joint level), and flattening ratio of MN (long axis/short axis); CT units of MN, flexor retinaculum (FR), and tendon; and bowing of transverse carpal ligament (TCL), length of the capitate, carpal arch width (CAW), carpal arch length (CAL), carpal arch area (CAA), and width and depth of carpal bony structures are shown in Table 1. Bland-Altman plots for the measurements showed good agreement between two independent observers (Figure-4).

The hamate hook level was chosen as the focal point for statistical analysis (*$P < 0.05$, **$P < 0.01$, ***$P < 0.001$). We classified carpal tunnel structures according to anatomic tendency, with category 1 showing steep changes (V- or

Table-1: The means ± SD of carpal tunnel structures at four levels.

	The distal radioulnar joint	The middle of the pisiform bone	The hamate hook	The proximal metacarpal bones
CSA of carpal tunnel (mm^2)	150.71 ± 37.35	142.06 ± 33.24	119.80 ± 21.28	146.79 ± 23.83
CSA of MN (mm^2)	7.15 ± 1.59	12.78 ± 3.36	15.47 ± 2.02	13.23 ± 2.59
Long axis of MN (mm)	3.31± 0.45	4.92 ± 0.85	6.19 ± 0.61	6.48 ± 0.75
Short axis of MN (mm)	2.33 ± 0.34	3.19 ± 0.53	3.35 ± 0.52	2.68 ± 0.44
Flattening ratio of MN	1.42 ± 0.15	1.59 ± 0.44	1.92 ± 0.41	2.57 ± 0.60
CT unit of FR (HU)	-0.27 ± 10.08	52.68 ± 15.40	75.01 ± 8.13	69.06 ± 10.48
Width of carpal tunnel bony structure (mm)		31.45 ± 3.22	23.06 ± 2.27	36.98 ± 3.88
Depth of carpal tunnel bony structure (mm)		11.50 ± 1.34	10.35 ± 0.85	8.06 ± 0.57
CT unit of MN (HU)	43.00 ± 7.47	52.98 ± 6.27	51.45 ± 7.77	52.34 ± 4.04
CT unit of tendon (HU)	99.10 ± 5.72	100.58 ± 3.91	96.49 ± 4.12	92.11 ± 3.79
CAW (mm)			18.55 ± 1.61	
CAL (mm)			19.84 ± 1.78	
CAA (mm^2)			20.71 ± 2.59	
Bowing of TCL (mm)			0.08 ± 0.92	
Swelling ratio of MN		1.79 ± 0.39		
Length of the capitate (mm)			21.35 ± 1.29	

Table-2: Correlation analysis among Category 1 values at four levels.

	The distal radioulnar joint				The middle of pisiform bone				The hamate hook				The proximal metacarpal bones			
	CSA of MN	Short axis of MN	CSA of carpal tunnel	Width of bony structure	CSA of MN	Short axis of MN	CSA of carpal tunnel	Width of bony structure	CSA of MN	Short axis of MN	CSA of carpal tunnel	Width of bony structure	CSA of MN	Short axis of MN	CSA of carpal tunnel	Width of bony structure
CSA of MN	1				1				1				1			
Short axis of MN	0.693**	1			0.809***	1			0.544*	1			0.652**	1		
CSA of carpal tunnel	0.198	0.171	1		0.771***	0.696**	1		0.646**	0.408	1		0.196	0.121	1	
Width of bony structure	NA	NA	NA	1	0.365	0.268	0.769***	1	0.362	-0.251	0.499*	1	0.051	-0.306	0.632**	1

*P < 0.05, **P < 0.01, ***P < 0.001; NA: Not Available.

Table-3: Correlation analysis among Category 2 values at four levels.

	The distal radioulnar joint			The middle of pisiform bone			The hamate hook			The proximal metacarpal bones		
	Flattening ratio of MN	Long axis of MN	Depth of bony structure	Flattening ratio of MN	Long axis of MN	Depth of bony structure	Flattening ratio of MN	Long axis of MN	Depth of bony structure	Flattening ratio of MN	Long axis of MN	Depth of bony structure
Flattening ratio of MN	1			1			1			1		
Long axis of MN	0.379	1		0.518*	1		0.629**	1		0.593**	1	
Depth of bony structure	NA	NA	1	-0.515*	0.116	1	-0.461*	-0.166	1	0.383	0.434	1

*P < 0.05, **P < 0.01, ***P < 0.001; NA: Not Available.

inverted V-shape) and category 2 increasing or decreasing gradually (Figure-5).

Correlation between carpal tunnel structures in category 1 (Table-2) and category 2 (Table-3) was examined at four levels. In both categories, intra-category correlation was mostly found at hamate hook level and middle level of pisiform, followed by the level of proximal metacarpal bone. At the distal radioulnar joint level, intra-category correlation was not obvious in either category. Correlation analysis between carpal bony and soft tissue structures at three levels is shown in Table-4. The greatest correlation between the widths of bony and soft tissue structures was found at hamate hook level and proximal metacarpal bones level, and the greatest correlation in the depth of carpal tunnel bony and soft tissue structures was found at hamate hook level and middle level of pisiform. Taken together, the bony and soft tissue structures of carpal tunnel reached the most obvious correlation at hamate hook level. Meanwhile, CSA of the carpal tunnel was correlated with width and depth of the bony structures at three levels.

Table-4: Correlation analysis between bony and soft tissue structures of carpal tunnel.

	Width of bony structures			Depth of bony structures		
	The middle of the pisiformis	The hamate hook	The proximal metacarpal bones	The middle of the pisiformis	The hamate hook	The proximal metacarpal bones
CSA of carpal tunnel	0.769***	0.499*	0.632**	0.586**	0.764***	0.465*
CSA of MN	0.365	0.362	0.051	0.519*	0.397	-0.183
Long axis of MN	0.145	0.398	0.649**	0.116	-0.166	0.434
Short axis of MN	0.268	-0.251	-0.306	0.597*	0.420	-0.275
Flattening ratio of MN	-0.147	0.361	0.628**	-0.515*	-0.461*	0.383
Swelling ratio of MN	0.263			0.232		
CAW		0.834***			0.203	
CAL		0.863***			0.273	
CAA		-0.064			-0.159	
Bowing of TCL		0.290			0.275	

*P < 0.05, **P < 0.01, ***P < 0.001.

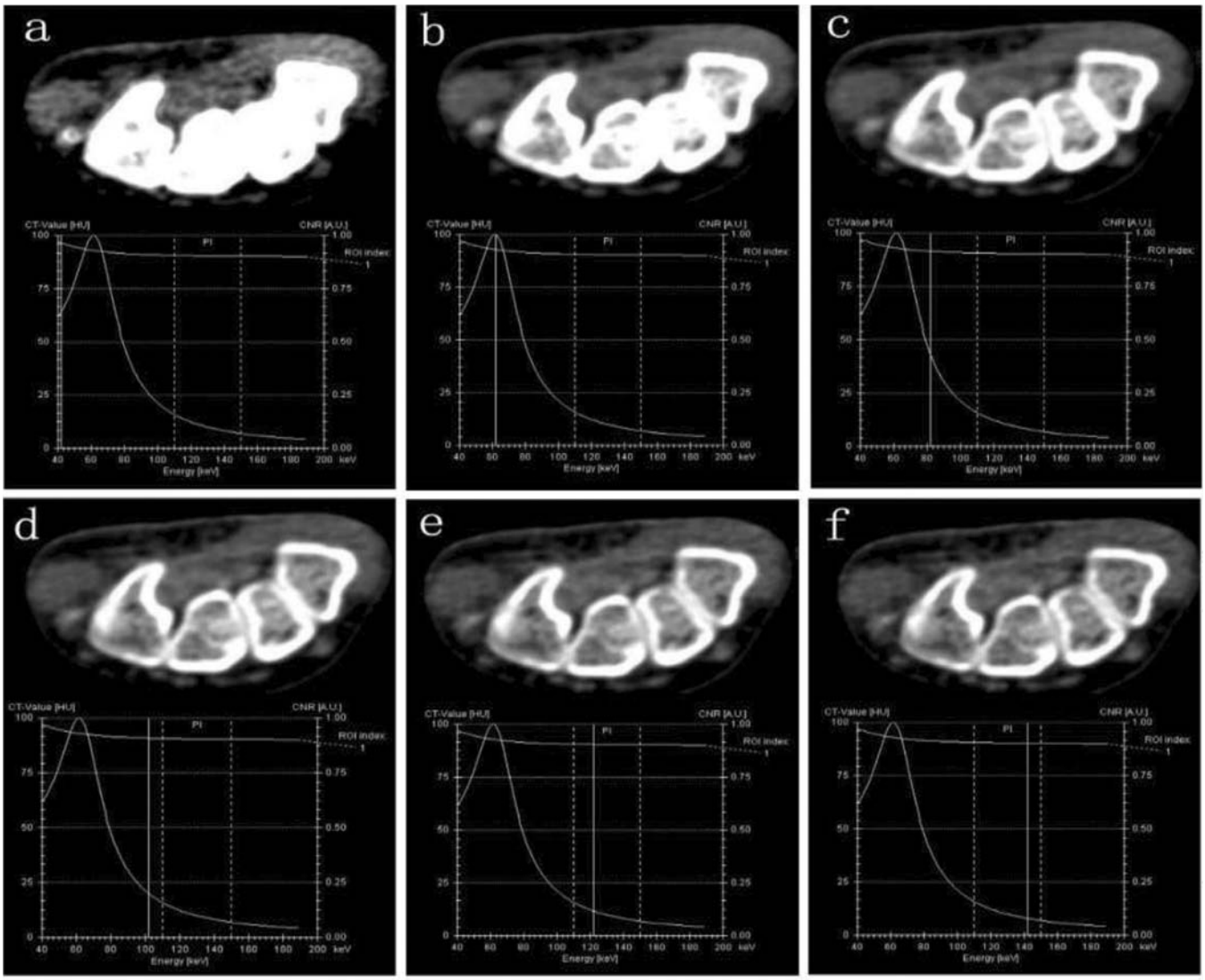

Figure-3: The images were reconstructed with 42 (a), 62 (b), 82 (c), 102 (d), 122 (e) and 142 (f) keV respectively, the best CNR through monoenergetic images was 62keV.

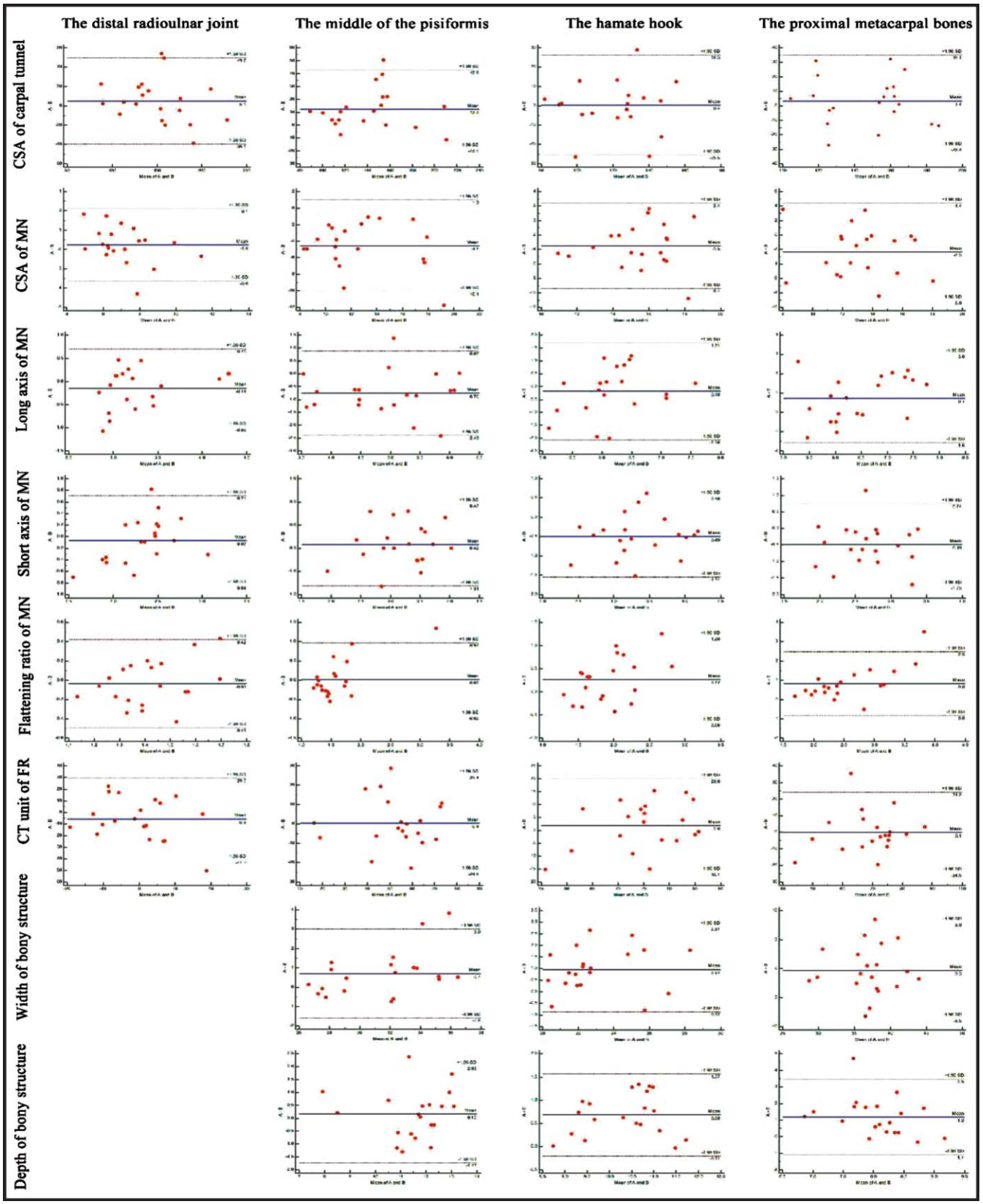

Figure-4: Bland-Altman plots demonstrated limits of agreement for carpal tunnel structures at four levels. A and B represented the two independent observer.

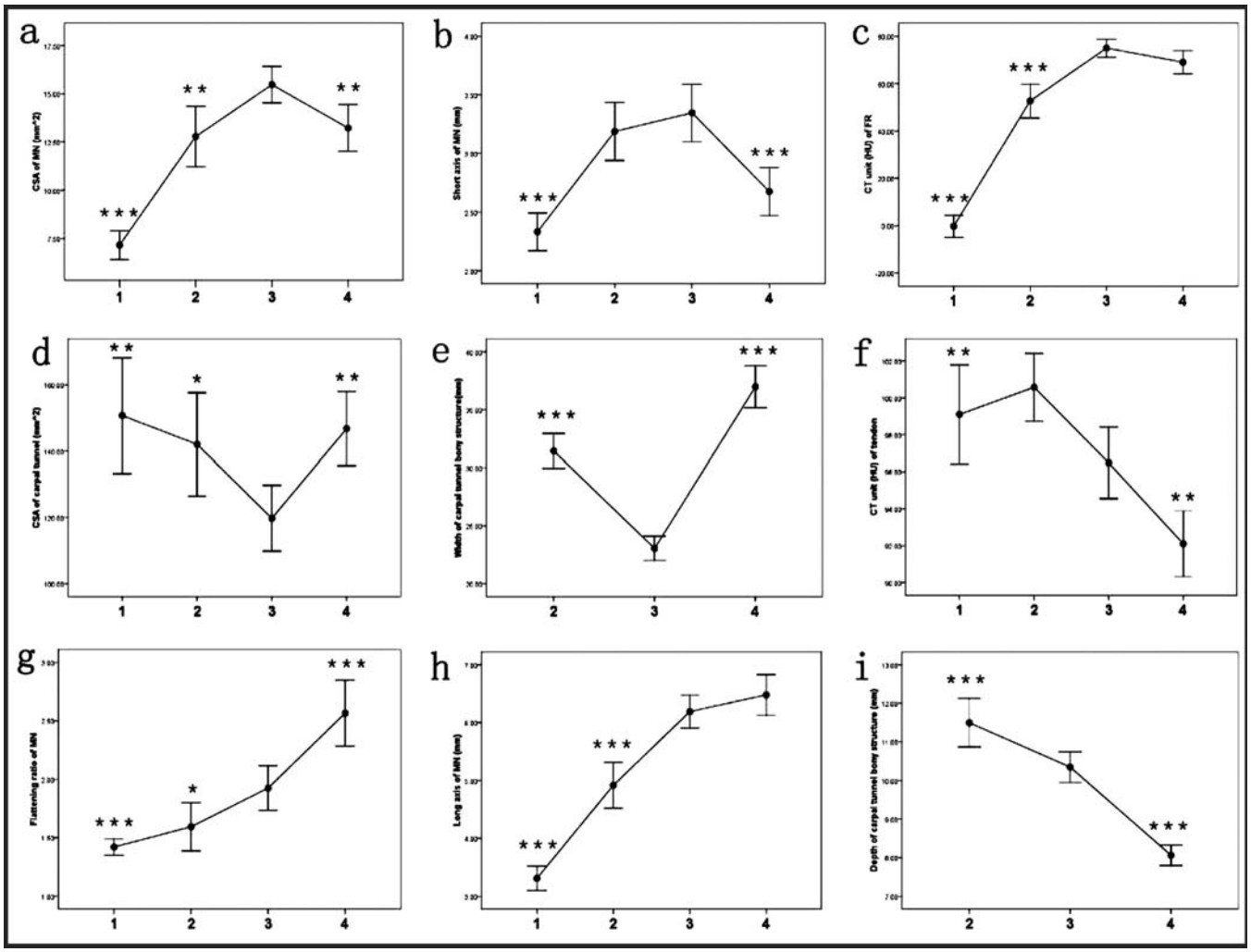

Figure-5: The number 1, 2, 3, 4 on the horizontal axis represented the level of the distal radioulnar joint, middle of the pisiformis, the hamate hook and the proximal metacarpal bones respectively. Anatomic tendency of CSA of MN, Short axis of MN, CT unit of FR, CSA of carpal tunnel, width of carpal tunnel bony structures, CT unit of tendon were shown in a, b, c, d, e, f respectively, we divided the above carpal tunnel structures as category 1, which resembled V-shape or inverted V-shape. g, h, i represented the anatomic tendency of flattening ratio of MN, long axis of MN, depth of carpal tunnel bony structures repectively, the above carpal tunnel structures were divided into category 2 that increased or decreased gradually.

Discussion

Significant improvements in image quality have been reported with monoenergetic techniques in a variety of tissues and organs, and corresponding optimal energy spectrum are also reported.[12,13] We hypothesized that this technique would also be useful for the structures of carpal tunnel. Images that were reconstructed at 62 keV had good inter-observer agreement in analysis, and we, therefore, recommend 62 keV as the optimal energy spectrum for monoenergetic DECT imaging of structures of carpal tunnel.

The MN is often compressed at hamate hook level due to regional stenosis, firm structure, and high pressure, and level of hamate hook has been a focal point in the study of CTS.[14] Thus, we chose this level as the basis for our statistical analysis.

The CSA of carpal tunnel was lowest at the level of hamate hook, and this finding was consistent with previous reports. Gabra et al found the CSA of carpal tunnel at hamate hook level was 20% less than that of other levels.[15] The anatomic tendency at CSA in our study was also consistent with the findings of Oge et al, who reported a similar anatomic tendency of CSA of carpal tunnel at MRI.[16] MRI has consistently shown that the smallest CSA of carpal tunnel is found at hamate hook level,[16] and it is thought that CSA at hamate hook level is more susceptible to pressure changes in carpal tunnel,[17] thus, this level should be a focal point in imaging

observation.

The FR can be divided into three successive segments: proximal slender segment, central firm segment and distal thin segment.[5] The FR was thickest at hamate hook level in a cadaver study,[18] and in our study, the highest CT number for FR was measured at hamate hook level, indicating that FR reached its greatest density at this level. We thought this might be because intra-tunnel tissues are more protected at the level of hamate hook.

Regarding MN, there are conflicting results as to CSA, as demonstrated by inconsistency in anatomic tendency and in the reporting of CSA at different levels. With respect to anatomic tendency, Monagle found that the change was not obvious,[19] while several other authors reported that MN assumed a "head-neck-body" morphology as it passed through carpal tunnel, with "neck" at hamate hook,[20] and still others argued that the tendency was more N-shaped and that the narrowest region was at the level of distal radioulnar joint.[21] In terms of quantitative assessments, the reported mean values of CSA of MN range from 8.6 mm^2 to 22.7 mm^2.[21-23] One reason for this wide variation might be that the small cross section creates difficulty in establishing optimal ROIs for measurements. Furthermore, the measurements could be affected by sample sizes and by the mode of imaging. In our study, anatomic tendency of MN resembled an inverted V, and the max CSA was at the level of hamate hook. Deniz et al considered CT inadequate for visualizing MN,[4] and although monoenergetic imaging might enhance visibility of MN, cross-sectional imaging of the nerve by DECT might still be insufficient.

The anatomic tendency of flattening ratio of MN was increased gradually. MRI findings have described flattening ratio of MN at each levels as: hamate hook > pisiform > distal radioulnar joint,[19] which is also approximately consistent with our findings. Collectively, the anatomic tendency of category 1 and 2 in our study was similar to that of most previous research. Thus, we believe DECT has a degree of potential for resolution of soft tissues of carpal tunnel.

In patients with CTS, morphological changes of carpal tunnel often occur at hamate hook level and middle level of pisiform bone.[14] Our finding that intra-category 1 and 2 correlation occurred mostly at hamate hook level and middle level of pisiform, suggested a clear correlation among morphological changes of intra-carpal structures at the two levels.

The morphology of carpal tunnel largely depends on carpal bony structures, and movement of carpal bones could partly change intra-carpal tunnel structures.[24] Displaced fractures and malalignment or deformity of carpal bones would change carpal tunnel volume and tend to elevate intra-carpal tunnel pressure, leading to entrapment of MN and contributing to CTS, which further demonstrated interplay between carpal bony and soft tissue structures.[25] Similarly, in cadaver specimens, carpal tunnel pressure increased with narrowing of carpal bony structures, while bowing of TCL and CSA of carpal tunnel at hamate hook level were forced to increase in order to accommodate the greater pressure, which again demonstrated the relationship between carpal bony structures and potential ability of carpal tunnel to expand under pressure.[17] In our study, carpal tunnel bony structures correlated with soft tissue structures, especially at hamate hook level. Furthermore, we found that CSA of carpal structures were all correlated with width and depth of bony structures at three levels. The CSA of carpal tunnel have been reported in association with CTS.[16] Hence, we surmised that the changes of carpal bony structures might be helpful in the diagnosis of CTS.

There were several limitations in this study. First, we did not use MRI images for reference, because our purpose was to study the anatomic tendency of adult carpal tunnel structures on DECT, rather than to verify the diagnostic efficiency of DECT. Second, all were young adults, and did not take into account variations in age, gender, height, weight, or handedness; besides, the study sample size was small. Third, although the total radiation dose of DECT is below the accepted threshold, it is still higher than that of SECT.

Conclusion

The optimal energy spectrum for imaging carpal tunnel structures by monoenergetic DECT was 62 keV. DECT permits a degree of visualization of soft tissues in carpal tunnel and was able to demonstrate the anatomic tendency of carpal tunnel structures. Carpal bony structures correlated with carpal soft tissue, and especially correlated with the CSA of carpal tunnel. As DECT technology evolves, we believe it has good prospects in clinical evaluation.

Disclaimer: None to declare.

Conflict of Interest: None to declare.

Funding Disclosure: This work was funded by the National Key Research and Development Programme of China (Grant No. 2016YFC0107102 (S. P.)), the National Natural Science Foundation of China (Grant No. 81271538 (S. P.)), Hunan Provincial Natural Science Foundation of

China (Grant No. 2017JJ2225 (J. L.)), Hunan Provincial Science and Technology Innovation Programme of China (Grant No. 2017SK50203 (H. Z.)). The funders had no role in study design, data collection and analysis, decision to publish, or preparation of the manuscript.

References

1. Festen-Schrier VJMM, Amadio PC. The biomechanics of subsynovial connective tissue in health and its role in carpal tunnel syndrome. J Electromyogr Kinesiol. 2018; 38:232-9.
2. Meraj S , Gyftopoulos S , Nellans K , Walz D , Brown MS, et al. MRI of the Extensor Tendons of the Wrist. AJR Am J Roentgenol. 2017; 209: 1093-102.
3. Chen YT, Williams L, Zak MJ, Fredericson M. Review of Ultrasonography in the Diagnosis of Carpal Tunnel Syndrome and a Proposed Scanning Protocol. J Ultrasound Med. 2016; 35:2311-24.
4. Deniz FE, Oksüz E, Sarikaya B, Kurt S, Erkorkmaz U, Ulusoy H, et al. Comparison of the diagnostic utility of electromyography, ultrasonography, computed tomography, and magnetic resonance imaging in idiopathic carpal tunnel syndrome determined by clinical findings. Neurosurgery. 2012; 70:610-6.
5. Ghasemi-Rad M, Nosair E, Vegh A, Mohammadi A, Akkad A, Lesha E, et al. A handy review of carpal tunnel syndrome: From anatomy to diagnosis and treatment. World J Radiol 2014; 6: 284-300.
6. Mallinson PI , Coupal TM , McLaughlin PD , Nicolaou S , Munk PL , Ouellette HA . et al. Dual-Energy CT for the Musculoskeletal System. Radiology. 2016; 281:690-707.
7. Kosmala A, Weng AM, Heidemeier A, Krauss B, Knop S, Bley TA, et al. Multiple Myeloma and Dual-Energy CT: Diagnostic Accuracy of Virtual Noncalcium Technique for Detection of Bone Marrow Infiltration of the Spine and Pelvis. Radiology.2018; 286:205-13.
8. Schmoee J, Dirrichs T, Fehrenbacher K , Tietz E, Hardt F, Schmid M, et al. Virtual Monoenergetic Images (VMI+) in Dual-Source Dual-Energy CT Venography (DSDE-CTV) of the Lower Extremity Prior to Coronary Artery Bypass Graft (CABG): A Feasibility Study. Acad Radiol. 2020; 27:1249-54.
9. Sun ZQ. Medical Statistics. 3rd edition. Beijing: People's Medical Publishing House, 2010.
10. Dong Y, Zheng S, Machida H, Wang B, Liu A, Liu Y, et al. Differential diagnosis of osteoblastic metastases from bone islands in patients with lung couldcer by single-source dual-energy CT: advantages of spectral CT imaging. Eur J Radiol. 2015; 84:901-7.
11. Linsen PVM, Coenen A, Lubbers MM, Dijkshoorn ML, Ouhlous M, Nieman K. Computed Tomography Angiography with a 192-slice Dual-source Computed Tomography System: Improvements in Image Quality and Radiation Dose. J Clin Imaging. 2016; 6:44.
12. Wichmann JL , Nöske EM, Kraft J, Burck I, Wagenblast J, Eckardt A, et al. Virtual monoenergetic dual-energy computed tomography: optimization of kiloelectron volt settings in head and neck couldcer. Invest Radiol. 2014; 49:735-41.
13. Lenga L , Albrecht MH, Othman AE, Martin SS, Leithner D, et al. Monoenergetic Dual-energy Computed Tomographic Imaging: Cardiothoracic Applications. J Thorac Imaging. 2017; 32:151-8.
14. Goss BC, Agee JM. Dynamics of intracarpal tunnel pressure in patients with carpal tunnel syndrome. J Hand Surg Am. 2010; 35:197-206.
15. Gabra JN, Kim DH, Li ZM. Elliptical Morphology of the Carpal Tunnel Cross Section. Eur J Anat. 2015; 19:49-56.
16. Oge HK, Acu B, Gucer T, Yanik T, Savlarli S, Firat MM, et al. Quantitative MRI analysis of idiopathic carpal tunnel syndrome. Turk Neurosurg. 2012; 22:763-8.
17. Li ZM, Masters TL, Mondello TA. Area and shape changes of the carpal tunnel in response to tunnel pressure. J Orthop Res. 2011; 29:1951-6.
18. Nanno M, Sawaizumi T, Kodera N, Tomori Y, Takai S, et al. Three-dimensional Analysis of the Attachment and Path of the Transverse Carpal Ligament. J Nippon Med Sch. 2015; 82:130-5.
19. Monagle K, Dai G, Chu A, Burnham RS, Snyder RE. Quantitative MR imaging of carpal tunnel syndrome. AJR Am J Roentgenol.1999; 172:1581-6.
20. Nakamichi KI, Tachibana S. Enlarged median nerve in idiopathic carpal tunnel syndrome. Muscle Nerve. 2000; 23:1713-8.
21. Jarvik JG, Yuen E, Haynor DR, Bradley CM, Fulton-Kehoe D, Smith-Weller T, et al. MR nerve imaging in a prospective cohort of patients with suspected carpal tunnel syndrome. Neurology. 2002; 58:1597-602.
22. Yao L, Gai N. Median nerve cross-sectional area and MRI diffusion characteristics: normative values at the carpal tunnel. Skeletal Radiol. 2009; 38:355-61.
23. Cha JG, Han JK, Im SB, Kang SJ. Median nerve T2 assessment in the wrist joints: preliminary study in patients with carpal tunnel syndrome and healthy volunteers. J Magn Reson Imaging. 2014; 40:789-95.
24. Mogk JP, Keir PJ. The effect of landmarks and bone motion on posture-related changes in carpal tunnel volume. Clin Biomech (Bristol, Avon) 2009; 24:708-15.
25. Niver GE, Ilyas AM. Carpal tunnel syndrome after distal radius fracture. Orthop Clin North Am. 2012; 43:521-7.